Precision Formation Delta-V Requirments for Distributed Platforms in Earth Orbit

Daniel P. Scharf, Fred Y. Hadaegh, and Scott R. Ploen

Jet Propulsion Laboratory
4800 Oak Grove Drive, Pasadena, CA USA

ABSTRACT

Distributed spacecraft flying in formation can overcome the resolution limitations of monolithic, Earth-sensing systems. However, formation spacecraft must now expend fuel to counteract disturbances and the gravity gradients between spacecraft. We consider three different formation architectures and determine the Δv required to maintain relative positions at accuracies from 0.1 to 10 m (1σ). The three architectures considered are: (*i*) Leader/Follower, in which individual spacecraft controllers track with respect to a passive, leader spacecraft, (*ii*) Center of Formation, in which individual spacecraft controllers track with respect to the geometric center of the formation, and (*iii*) Iterated Virtual Structure, in which a formation template is fit each timestep and individual spacecraft controllers track with respect to the fitted template. We show that in the presence of relative and inertial sensor noise and disturbances such as Earth oblateness and aerodynamic drag, relative positions can be maintained to the 10 m level for 4 $mm/s/orbit$.

Keywords: Formation Flying, Control Architectures, Planetary Orbit, Delta-V Requirements

1. INTRODUCTION

By using a number of small spacecraft in place of a large deployable antenna, sparse and synthetic apertures from hundreds of meters to kilometers can be realized for Earth imaging. The Cold Land Process Research Mission (EX-7) and the Topography and Surface Change Mission (EOS-8) are two missions considering distributed spacecraft interferometric synthetic aperture radars (InSAR). There are also several proposed topographic InSAR formations, where small receiver satellites fly in formation with a larger, monolithic SAR transmitter/receiver.[1] In addition to enabling large synthetic apertures, spacecraft formations offer launch and deployment efficiency, are straightforward to upgrade, have a graceful degradation of science capability with failures, and avoid the structural complexity and pointing issues associated with large flexible antennas.

There are, of course, trade-offs. The most important is that individual spacecraft must now expend fuel to maintain a specific configuration of relative positions. Fuel is needed both to reject differential disturbances that would disperse the formation and to cancel gravity gradients that result from the spatial configuration of the formation. Even in the absence of disturbances, arbitrary configurations can require a delta-v (Δv) of up to 7 $m/s/orbit$ to maintain, which is clearly impractical.[2,3]

As a result, there has been considerable research into scientifically-useful *passive relative orbits* (PROs), which are thrust-free, periodic relative spacecraft trajectories.[3] Rather than cancelling the natural dynamics with control effort (i.e., fuel), on PROs formation spacecraft use the dynamics to their advantage. By careful selection of PROs and formation control design, studies have shown that for a 600 m diameter formation in a 500 km orbit relative positions can be controlled to an accuracy of 10 meters for approximately 7 mm/s per orbit of Δv.[4,5] This amount of Δv is practical.

In addition to PRO selection, control design significantly affects formation Δv requirements. Formation control design is a two step process: first a formation control architecture is selected and then control algorithms are designed within the architecture's constraints. A control architecture specifies the overall coordination strategy of a formation, that is, how the spacecraft are coupled through control. There are three architectures

Send correspondence to Daniel P. Scharf
E-mail: Daniel.P.Scharf@jpl.nasa.gov, Telephone: 1 818 354 4795

generally considered: (*i*) Multiple-Input Multiple-Output (MIMO), in which the formation is treated as a single multiple-input, multiple-output plant, (*ii*) Leader/Follower (L/F), in which individual spacecraft controllers are connected hierarchically, and (*iii*) Cyclic, in which individual spacecraft controllers are connected non-hierarchically.[6]

Once a formation control architecture is selected, then the underlying control algorithms are designed. Consider an L/F arrangement of two spacecraft maintaining their position with respect to a third, passive spacecraft. An optimal multiple-input, multiple-output methodology, such as the linear quadratic regulator (LQR), can be used to design separate controllers for each active spacecraft. As another example, in Ref. 4 an optimal model predictive controller (MPC) is used.

Initial studies for deep space formations by the authors and Earth-orbiting studies by others have shown that the Δv required to achieve a given relative position control accuracy can vary by up to 50% with control architecture.[5,7] An additional savings of 50% in Δv is possible depending on PRO selection.[4]

The performance studies done by Tillerson, How and co-workers[4,5,8] focused on two particular formation control architectures: Leader/Follower and a type of Cyclic architecture called Virtual Center. These studies used an optimal MPC control algorithm design methodology. The purpose of this paper is to complement and extend these earlier studies to (*i*) an additional control architecture (another type of Cyclic architecture called Iterated Virtual Structure), (*ii*) an additional control algorithm design methodology (LQR), (*iii*) different relative position control accuracies (including sub-meter), and (*iv*) inertial position uncertainties. For each of these cases, we compare the Δv required to achieve the various control accuracies.

Performance, however, is not the only consideration in selecting a control architecture. Robustness and the amount of inter-spacecraft communication and sensing required also affect mission cost. Communication and relative sensing requirements are heavily dependent on formation estimator design,[9,10] and quantifying these aspects are beyond the scope of this paper. We do discuss the robustness properties of the control architectures considered.

The remainder of this paper is organized as follows. In the next section, we discuss PROs in more detail and describe the PRO used in this study. Then design considerations for orbit control via LQR are presented. Next, three representative formation control architectures are introduced. After discussing the simulation environment, the main results of the Δv simulation study are presented. Finally, we summarize and identify areas for future work.

2. PASSIVE RELATIVE ORBITS

In the following we refer to the Local-Vertical, Local-Horizontal (LVLH) frame of an orbit, defined as follows: the x direction is along the radial vector, the z direction is normal to the instantaneous orbit plane, and the y direction completes the triad. The x, y and z directions are also commonly referred to as radial, along track and cross track.

Passive relative orbits (PROs) are thrust-free solutions to models of relative spacecraft dynamics. The simplest example of a PRO is an elliptical, homogeneous solution to the Hill-Clohessy-Wiltshire (HCW) equations.[2,11,12] The HCW equations result from considering an ideal gravitational primary, linearizing about a circular reference orbit, and representing the dynamics in the LVLH frame of the reference orbit. Periodic solutions of the HCW equations that are not offset from the origin of the LVLH frame have the following form

$$\begin{aligned} x(t) &= \frac{1}{2}\rho_1 \cos(nt + \phi_1) \\ y(t) &= \rho_1 \sin(nt + \phi_1) \\ z(t) &= \rho_2 \cos(nt + \phi_2) \end{aligned} \tag{1}$$

where n is the mean motion of the reference orbit (i.e., average angular rate of the orbit), and ρ_1, ρ_2, ϕ_1, and ϕ_2 are constants determined from initial conditions.[13] These solutions are referred to as Free Elliptical Trajectories (FETs).

For an Earth-imaging synthetic aperture, a combiner spacecraft can be placed on the reference orbit and collector spacecraft placed on the same FET with different phasing. The natural dynamics then cause the collector spacecraft to travel around the central combiner, thereby providing multiple baselines.[2] A FET of particular interest is the Circular Projected Free Elliptical Trajectory (CPFET),[2,14] which projects a circle onto the y-z plane. This plane is parallel to the surface of the Earth. By setting $\rho_1 = \rho_2$ and $\phi_1 = \phi_2 = 0$ in (1), it can be shown that the CPFET resides in a plane rotated $\pm 26.56°$ about the y-axis.

These elliptic, homogeneous solutions do not exist in reality; oblateness, aerodynamic drag or even a small amount of uncorrected eccentricity in the reference orbit will destroy the periodicity of these HCW solutions. If a formation spacecraft is required to follow a homogeneous HCW solution, it will consume fuel maintaining a PRO that does not exist in reality.[15]

Ref. 15 considers a spacecraft actively following a FET, but where the reference orbit has an eccentricity of 0.005 (i.e., not 0). It is shown that the Δv required to follow the FET is more than is required to reject the disturbance caused by the oblateness of the Earth.

The closer a model of the relative spacecraft dynamics is to reality, the less Δv will be required in practice to follow a periodic solution of the model. In this study we consider a PROs that exists in a more complex model than the HCW equations: an approximate-CPFET that exists about an eccentric reference orbit and that is useful for synthetic aperture imaging.

The parameters for the reference orbit and the PRO for each spacecraft (SC) are included in Tables 1 and 2 at the end of this section. We consider three spacecraft with one approximately in the center of the formation that serves as a reference spacecraft for sensing and navigation. Two other spacecraft move relative to the reference spacecraft. While a reference LVLH frame is used for PRO design, due to disturbances the first, reference spacecraft does *not* remain at the origin of the LVLH frame. The reference spacecraft does not need to be near the center of the formation, although this does simplify some calculations.

PROs in even more complex models have been considered, such as in linearized and nonlinear models with both reference orbit eccentricity and Earth oblateness. However, these more complex PROs have not yet been associated with science applications and have a more limited design space. Further, the modified-CPFET has been used in previous Δv studies and serves as a baseline for comparison.

2.1. Approximate CPFET for Eccentric Reference Orbit

As mentioned previously, for mildly eccentric orbits such as the Space Shuttle's orbit ($e = 0.005$), the effects of eccentricity dominate those of Earth oblateness when trying to follow an HCW equation PRO.[15] Therefore, one avenue for developing a PRO closer to reality is to include reference orbit eccentricity.

Linearizing about an eccentric reference orbits results in a time-varying system. By considering derivatives with respect to the reference orbit true anomaly θ instead of time, the following closed form homogeneous solution can be obtained for motion relative to an eccentric orbit[15]:

$$\begin{bmatrix} x \\ y \\ \frac{dx}{d\theta} \\ \frac{dy}{d\theta} \end{bmatrix} = \begin{bmatrix} es & 2e^2sH(\theta) - \frac{ec}{(1+ec)^2} & -c & 0 \\ 1+ec & 2eH(\theta)(1+ec) & s\left(1+\frac{1}{1+ec}\right) & \frac{1}{1+ec} \\ ec & 2e^2cH(\theta) + \frac{es}{(1+ec)^2} & s & 0 \\ -es & \frac{2ec}{(1+ec)^2} - 2e^2sH(\theta) & c\left(1+\frac{1}{1+ec}\right) + \frac{es^2\theta}{(1+ec)^2} & \frac{es}{(1+ec)^2} \end{bmatrix} \begin{bmatrix} d_1 \\ d_2 \\ d_3 \\ d_4 \end{bmatrix}$$

$$\begin{bmatrix} z \\ \frac{dz}{d\theta} \end{bmatrix} = \begin{bmatrix} \frac{s}{1+ec} & \frac{c}{1+ec} \\ \frac{e+c}{(1+ec)^2} & \frac{-s}{(1+ec)^2} \end{bmatrix} \begin{bmatrix} d_5 \\ d_6 \end{bmatrix} \tag{2}$$

where e is the eccentricity of the reference orbit, c is $\cos\theta$, s is $\sin\theta$, the d_i are constants that depend on initial conditions, and

$$H(\theta) = -(1-e^2)^{-5/2}\left[\frac{3}{2}eE - (1+e^2)\sin E + \frac{1}{2}e\sin E\cos E + d_H\right] \tag{3}$$

where E is the eccentric anomaly of the reference orbit and d_H is a constant such that $H(\theta_0) = 0$, where θ_0 is the initial true anomaly. If $\theta_0 = 0$, then $d_H = 0$.

Ref. 15 considers PROs about eccentric reference orbits in detail. Summarizing, the periodicity condition, that is, the condition for a PRO, is $d_2 = 0$. To see this, consider that the only unbounded term in (3) is $H(\theta)$. This unboundedness is due to the eccentric anomaly, which is *not* limited to the range $[0, 2\pi)$. Equivalently, if $\theta_0 = 0$, then $d_2 = 0$ if

$$\frac{dy}{d\theta}(0) = -\frac{2+e}{1+e}x(0)\,. \tag{4}$$

The approximate-CPFET we consider is initialized at $\theta_0 = 0$ with the reference spacecraft on the reference orbit. CPFET initial positions are used even though the CPFET does not exist in a model with reference orbit eccentricity. However, by using CPFET initial positions and the periodicity condition for an elliptic reference orbit, an approximate-CPFET is obtained for smaller eccentricities.

In the previous study by Tillerson et al.,[5] an approximate-CPFET with a radius of 300 m was considered. Therefore, we initialize the second spacecraft's position with an actual CPFET's initial conditions at maximum positive z displacement and the velocity based on (4):

$$\begin{bmatrix} x & y & z \end{bmatrix} = \begin{bmatrix} 335.4\sin 26.56^\circ & 0 & 335.4\sin 26.56^\circ \end{bmatrix} \; m$$
$$\begin{bmatrix} \frac{dx}{d\theta} & \frac{dy}{d\theta} & \frac{dz}{d\theta} \end{bmatrix} = \begin{bmatrix} 0 & -\frac{2+e}{1+e}x(0) & 0 \end{bmatrix} \; m/rad \tag{5}$$

With these initial conditions, the projection of the PRO on the $y - z$ plane is very close to circular. The third spacecraft is initialized opposite the second to the CPFET initial position at maximum negative z displacement. A plot of the approximate-CPFET is shown in Figure 1.

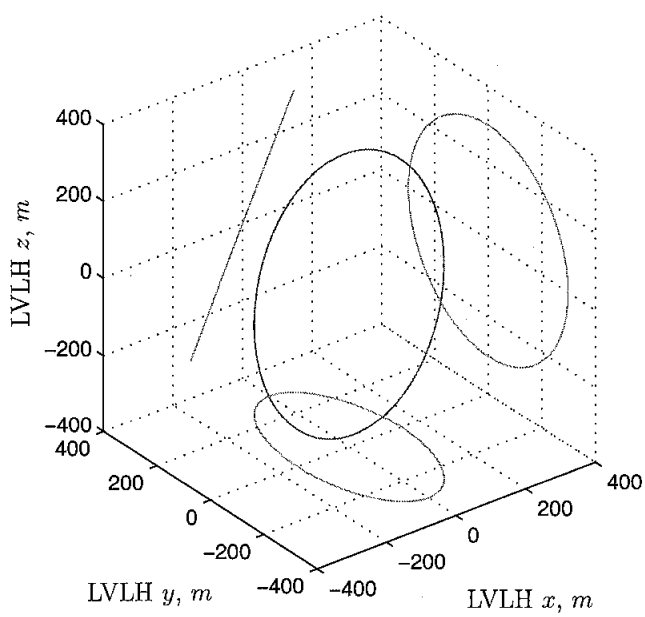

Figure 1. Approximate CPFET, $e = 0.005$

By selecting the maximum z displacements at $\theta_0 = 0$ the spacecraft have the maximum possible difference in inclination. This inclination difference is important since the differential effect of Earth oblateness is maximized. That is, the primary disturbance is at its largest. Placing the spacecraft at zero z displacement would have resulted in a longitude of the ascending node difference. As a result, all spacecraft would be disturbed by oblateness, but the differential disturbance would be zero.

For formation control, first a desired trajectory is specified via the d_i of (2). Then, given a θ, the desired location of a spacecraft relative to a reference point can be determined. In the sequel, we discuss both the selection of θ and the reference point.

The initial conditions for the PRO in the simulations are given in the following tables.

Table 1: Reference Orbit for PRO Design.

Orbital Element	Value
Semi-major Axis	6900 km
Eccentricity	0.005
Inclination	35°
Longitude of the Ascending Node	0°
Argument of Perigee	0°
True Anomaly	0°

Table 2: PRO Constants for Spacecraft.

	SC 1 (km)	SC 2 (km)	SC 3 (km)
d_1	0	0	0
d_2	0	0	0
d_3	0	-0.1500	0.1500
d_4	0	0	0
d_5	0	0	0
d_6	0	0.3015	-0.3015

Having discussed the PROs that the formation spacecraft follow, we now review the LQR design methodology used to design the formation control algorithms.

3. LINEAR QUADRATIC REGULATION

Regardless of the formation control architecture selected, the LQR design methodology is identical. What varies among architectures is the control design model, the reference point for the PRO and the reference θ. For our application of LQR, a discrete linear time-invariant model of the form

$$\dot{x}_{k+1} = A_d x_k + B_d u_k \tag{6}$$

is needed, where x_k is the state (not to be confused with the LVLH x coordinate) at the kth time step and u_k is the control input. The standard optimal steady-state LQR controller is then given by $u_k = -Gx_k$ where $G = (B_d^T S B_d + R)^{-1} B_d S A_d$, S is the solution to the algebraic Riccati equation

$$S = A_d^T [S - SB_d(B_d^T S B_d + R)^{-1} B_d^T S] A_d + Q\,, \tag{7}$$

and Q and R are weighting matrices.[16] This G minimizes the cost $J = \int_0^\infty x^T Q x + u^T R u dt$ subject to (6). For initial studies, typical values for Q and R are the identity matrix and λ times the identity matrix, respectively. The parameter λ is used to weight control effort (cost) versus state error (performance).

For LQR, the control design model must be time-invariant. The PRO design model is time varying, and so a different model must be used for LQR control design. Based on the results in Ref. 4, we use a model of the relative spacecraft dynamics linearized about a circular reference orbit and augmented with the effects of oblateness. This "oblate-HCW" model modifies the frequencies of motion planar (x/y) and out-of-plane (z) motion. The control design model in continuous time is from Ref. 17:

$$\begin{aligned} \ddot{x} - 2nc\dot{y} - (5c^2 - 2)n^2 x &= a_x \\ \ddot{y} + 2nc\dot{x} &= a_y \\ \ddot{z} + (3c^2 - 2)n^2 z &= a_z \end{aligned} \tag{8}$$

where n is again the mean motion of the circular reference orbit, the a_i are constant disturbance and control accelerations and $c = \sqrt{(1+s)}$, where

$$s = \frac{3}{8} J_2 \frac{R_e^2}{a_r^2}(1 + 3\cos 2i_r) \tag{9}$$

and R_e is the radius of the Earth, J_2 is the second zonal harmonic, and i_r and a_r are inclination and semi-major axis, respectively, of the circular reference orbit. For this study we ignore the constant disturbances in the a_i,

but they can be fed forward—LQR does not incorporate constant disturbances explicitly. The z motion can be further augmented as well, but this requires either an iterative process not suitable in a control design model or making approximations based on a specific PRO geometry.

The continuous time model of (8) must be transformed to a discrete time model. If the continuous time model is given by $\dot{x} = Ax + Bu$, then the discretized model has

$$A_d = e^{AT_s} \quad \text{and} \quad B_d = \int_0^{T_s} e^{A(T_s-\tau)} B d\tau$$

where T_s is the sample time of the controller. To calculate B_d, a time dependence for $u(\cdot)$ has been assumed, namely, a zero order hold where u is constant over T_s. However, for orbit control this assumption is not feasible; the spacecraft would always be thrusting. We assume that u is constant over an interval of length σT_s, where $\sigma \in (0, 1]$. Then the equation for B_d is

$$B_d = \int_0^{\sigma T_s} e^{A(T_s-\tau)} B d\tau.$$

The parameter σ is a design variable in addition to λ and T_s.

The state transition matrix for the continuous time control design model (8) can be obtained in closed form. This in turn is used to find closed forms of A_d and B_d. These matrices are included in the Appendix.

Finally, note that while (8) and its discrete counterpart model the dynamics of a spacecraft relative to a reference orbit, the model for the dynamics of two spacecraft in the vicinity of the reference orbit is identical. Therefore A_d and B_d embody the dynamics of $SC\ j$ with respect to the reference orbit and with respect to $SC\ i$. While the model is the same, it is crucial that the states be represented in the correct LVLH frame. For relative control of $SC\ j$ with respect to $SC\ i$, the LVLH frame of $SC\ i$ must be used.

4. FORMATION CONTROL ARCHITECTURES

Three control architectures were identified in the Introduction: (*i*) Multiple-Input Multiple-Output (MIMO), in which the formation is treated as a single multiple-input, multiple-output plant, (*ii*) Leader/Follower (L/F), in which individual spacecraft controllers are connected hierarchically, and (*iii*) Cyclic, in which individual spacecraft controllers are connected non-hierarchically. In this study we consider L/F and two Cyclic architectures: Center of Formation (COF) and Iterated Virtual Structure (IVS). For a three spacecraft formation the MIMO architecture is not appreciably different from the L/F architecture when LQR is used as a design algorithm. Hence, MIMO is only briefly discussed.

4.1. MIMO

In a MIMO architecture the relative states of a formation are considered as a single plant, and a multiple-input, multiple-output control design methodology is used.

To use the LQR design methodology, a control design model is need that includes all the linearly independent relative states. We select the relative state between SC 1 and SC 2, and between SC 1 and SC 3. These relative dynamics are identical. As a result, the MIMO LQR design model corresponding to (6) is

$$x_{k+1} = \begin{bmatrix} A_d & 0 \\ 0 & A_d \end{bmatrix} x_k + \begin{bmatrix} B_d & 0 \\ 0 & B_d \end{bmatrix} u_k \tag{10}$$

where the state is $[\, x_{12}\ y_{12}\ z_{12}\ \dot{x}_{12}\ \cdots\ x_{13}\ \cdots\ \dot{z}_{13}\,]^T$, the relative states x_{12}, $x_{13}\, y_{12}$, etc. are in the LVLH frame of SC 1, and $u_k = [\,(u_2 - u_1)^T \quad (u_3 - u_1)^T\,]^T$, where u_i is the control acceleration applied to $SC\ i$ at timestep k.

For Q equal identity and R equal λ times identity, the resulting gain matrix G is block diagonal. That is, LQR generates two decoupled controllers: one for the relative state between SC 1 and SC 2, and one for the relative state between SC 1 and SC 3. As is seen in the next section, this control design is identical to the

Leader/Follower LQR formation control design *for this formation.* For larger formations with more complex Leader/Follower architectures, the MIMO and L/F designs are not identical.

For this small formation, the MIMO architecture design can still be made different by also weighting the relative state between SC 2 and SC 3 in the Q matrix.[18] Then a non-identity Q matrix and a non-block diagonal G matrix are obtained. However, for the three spacecraft formation considered in this study, the difference between the MIMO and L/F controllers is not appreciable, and so we do not study the performance of the MIMO formation controller in simulation.

There are two remaining items of note. First, SC 1's control is free in (10). As suggested in by Smith and Hadaegh,[19] a linear programming problem can be solved to minimize the overall control effort of the formation. Specifically, given the controller output $u_2 - u_1 = a_1$ and $u_3 - u_1 = a_2$ at timestep k, solve

$$\min_{u_1} \sum_{i=1}^{3} \|u_i\|_1$$

$$\text{subject to} \quad \begin{array}{l} u_2 - u_1 = a_1 \\ u_3 - u_1 = a_2 \end{array} .$$

The second item of note is that MIMO architecture formation controllers are generally not structurally robust. Specifically, if a thruster fails, the entire formation can become unstable. In Leader/Follower, only the spacecraft with the failure (and its followers) are affected. In Cyclic architectures, the behavior is more complex, but generally the formation is maintained with the failed member.

4.2. Leader/Follower

As the name suggests, in Leader/Follower (L/F), spacecraft are assigned to follow other spacecraft, with at least one spacecraft in the formation not following any other spacecraft. The key aspect of L/F is that the follower assignment must be such that for every spacecraft, it is not possible to follow a chain of followers back to it. This constraint maintains the hierarchical structure of the control dependencies. As a result, when all spacecraft follow a single leader the formation is stable if the individual tracking controllers of each spacecraft are stable. L/F reduces formation control design to decoupled tracking controller designs.

For the three spacecraft formation considered in this study, SC 1 is the sole leader, and SC 2 and SC 3 both follow it independently. As such, the LQR control design model is simply

$$x_{k+1} = A_d x_k + B_d(u_i - u_1) \tag{11}$$

where the state is the relative state between SC 2 or 3 and SC 1. Since the relative dynamics are identical, the controller for each follower is identical.

Note that u_1 is again free. The same minimization problem as was posed in the MIMO architecture can be used in the L/F architecture. While this may appear to violate the strict, hierarchical requirement of L/F, the closed-loop relative dynamics between each follower and the leader are identical to the case where $u_1 = 0$. If, however, there are multiple layers of followers, the minimization problem must include all followers, and the communication requirements approach those of a MIMO architecture.

There are several methods for specifying the desired true anomaly θ that is used to determine the desired positions of the followers via (2) and the constants in Table 2. Using the true anomaly of the reference SC 1 led to a larger error than using a prescribed, model-based true anomaly. We hypothesize that this is due to the perturbation effects of Earth oblateness. Using the true anomaly of a purely Keplerian reference orbit was found to produce a smaller open loop tracking error by an order of magnitude. However, due to oblateness, the open loop tracking error with a prescribed true anomaly has a secular term. To counteract this, the reference orbit is reset to the state of SC 1 at the beginning of each orbit. This reset is done with inertial sensor noise included, that is, the orbital elements of SC 1 are not known exactly.

4.3. Cyclic

In a Cyclic architecture, individually designed spacecraft controllers are connected non-hierarchically. The hierarchical control dependencies of the Leader/Follower architecture lead to straightforward stability results. When the a hierarchical arrangement is not maintained, additional layers of feedback are introduced that make stability analysis difficult. Most Cyclic controllers are analyzed through extensive simulation.

However, Cyclic architectures blend the performance advantages of MIMO architectures with the robustness of L/F architectures. We study two types of Cyclic architecture that couple the individual spacecraft controllers in different ways. The first is referred to as Center of Formation (COF) control in which the all spacecraft control with respect to the geometric center of the formation. Given desired and actual relative positions, COF minimizes the tracking error of the formation in a least squares sense. COF has its roots in the centroiding strategies in the robotics literature,[20] and has been generalized to include a weighted center in Ref. 5, where it is referred to as Virtual Center. The weighting matrix can be based on remaining fuel, in which case the weighted center allocates larger tracking errors to fuel-rich spacecraft. In COF, control design is still independent, but all spacecraft are coupled through the calculation of the geometric center: in effect, every spacecraft feeds back the relative state of every other spacecraft.

The second Cyclic architecture is referred to as Iterated Virtual Structure (IVS),[6] and it is a further generalization of COF. Each time step the formation "template," that is, the desired shape of the formation, is fit in both orientation and position to the current spacecraft locations to minimize a measure of the tracking error. COF only fits the position of the template. For our three-spacecraft formation, the desired true anomaly θ is the orientation of the template. It is fitted to minimize the tracking error with respect to the geometric center of the formation. For this preliminary study, we have separated the coupled problem template fitting problem: first the position of the template is placed at the geometric center, and then the orientation of the formation template, which in our case is θ, is fit.

There are no analytic stability guarantees for any of these Cyclic architectures, but simulation studies have shown built confidence in these architectures.

For both the COF and IVS architectures, the same LQR controller is used by each spacecraft as is used in the L/F architecture, with an additional, identical controller for SC 1. However, the spacecraft do not control with respect to a leader, but with respect to the geometric center of the formation. For COF, the desired true anomaly for calculating the PRO is the prescribed as it is for L/F. For IVS, Brent's method is used to find the true anomaly that minimizes the tracking error starting with SC 1's true anomaly as calculated with sensor noise.

5. SIMULATION ENVIRONMENT

A closed loop simulation environment was developed in Matlab to evaluate the Δv needed to achieve different levels of relative control performance. The dynamics includes Earth oblateness, aerodynamic drag with constant density and a moving atmosphere, and lunar and solar perturbations. Positions and velocities are recorded every 100th of an orbit. For the reference orbit in Table 1, this corresponds to every 57 s. Control is applied every T_s seconds, which is a multiple of the base rate of 57, seconds for σT_s seconds. The control accelerations are not quantized.

Ballistic coefficients of 0.005, 0.0025 and 0.0075 m^2/kg were used, resulting in differential drag accelerations of approximately $5 \times 10^{-8}\, m/s^2$. This level of differential drag matches the earlier study.[4]

White relative sensor noise of $2\,cm\,1\sigma$ and $0.46\,mm/s\,1\sigma$ and white inertial sensor noise of $10\,m\,1\sigma$ and $0.22\,m/s\,1\sigma$ was included in all measurements. With the exception of the inertial velocity noise, these noise levels are consistent with wide-area augmented GPS for inertial sensing[21] (i.e., with respect to the Earth) and carrier differential GPS for relative sensing.[22] The inertial velocity noise was obtained by using the relative sensing ratio of velocity to position noise. Also, we do not limit the noise in magnitude to the $1\,\sigma$ value as was done in previous studies. Note that the relative sensor measurements are made in the Earth-inertial frame. These measurements must be transformed to the LVLH frame of the reference spacecraft.

The inertial sensor noise introduces errors into the calculated instantaneous orbital elements of the reference SC 1. This uncertainty has two deleterious effects. First, the desired true anomaly used to calculate the desired relative positions of the spacecraft is in error. Second, the transformation of the inertial relative sensor measurements to the LVLH frame of the reference spacecraft has errors. These errors must be corrected by the formation controller.

5.1. Simulation Results

For each control architecture, ten orbits of closed-loop control was simulated, and the relative position control performance and Δv used were calculated. The relative position control performance is calculated as follows. Regardless of the control architecture, the tracking error for a spacecraft is the difference between its desired position with respect to the reference spacecraft and its actual position. The performance for a given spacecraft is the root-sum-square (RSS) of the means and variances of that spacecraft's tracking errors in each axis. The formation performance is the maximum of the spacecraft performances. Maximum control accelerations were also recorded.

In addition, the LQR design methodology has three design parameters: T_s, σ and λ. As λ, the control weighting, is varied, there is a trade-off between performance and Δv. The parameters T_s and σ were also found to significantly affect performance. Therefore, for each control architecture, a suite of specific LQR controllers was simulated. The suite of controllers was the same for all architectures, and it is shown in Table 3. In total, three control architectures (L/F, COF, and IVS) are each simulated with 36 different controllers each.

Table 3: Suite of LQR Design Parameters Simulated.

Parameter	Value
Sample Frequency ($1/T_s$)	$\{1/10^{th}, 1/50^{th}, 1/100^{th}\}$ of an orbit
Actuation Period σT_s	$\{0.1, 1, 10\}$ s
Control Weight λ	$\{1 \times 10^3, 1 \times 10^5, 1 \times 10^8, 1 \times 10^{10}\}$

The results for the L/F architecture are shown in Figures 2–5. The first three figures are for different actuation periods σT_s. Each figure has separate lines for each sample frequency. The control weight is varied to obtain each line. The best performance and highest Δv's correspond to the minimum λ. Similarly, the smallest Δv's correspond to the largest λ. Different sample frequencies are indicated by different line types (e.g., dashed or solid) and different actuation periods are indicated by different data point shapes (e.g., circle or triangle). In Figures 2–4 the maximum acceleration in mm/s^2 is stated next to each data point. The one value of 0.0 that appears indicates that the maximum acceleration was less than 50 $\mu m/s^2$. Figure 5 shows the results for all actuation periods on the same plot. It is a dense plot, and its purpose is to give an overall impression of the results for the L/F architecture. Note that each plot has a different abscissa and range.

The corresponding plots for COF and IVS performance are qualitatively similar. Table 4 summarizes the Δv requirements for different performance levels for each architecture. The Δv reported for each architecture is the minimum Δv of each architecture's 36 controllers.

From Table 4, IVS is clearly seen to be far superior to both L/F and COF. COF is approximately 15% more efficient than L/F, except at the $5\,m$ performance level. We believe this is an aberration due to the low number of values for λ. The lines in Figure 2 are concave. As more values of λ are simulated, the Δv required for a given performance level will decrease. Averaging over more orbits would also be beneficial.

From Table 4 we see that it is critical for Earth-orbiting formations to modify the desired formation trajectory in the presence of disturbances that do not exist in the PRO design model. When the desired trajectory is fit to the current formation geometry in IVS, dramatic Δv and fuel savings result.

Compared to the previous study in which 10 m absolute performance was maintained for 6.9 $mm/s/orbit$ using a COF architecture with an optimal model predictive controller, COF with LQR maintains 10 m absolute performance (approx. 3.3 $m\,1\sigma$) for 13.4 $mm/s/orbit$, but this value includes the effects of inertial sensor noise and white relative sensor noise. Removing inertial sensor noise and limiting the relative sensor noise magnitudes

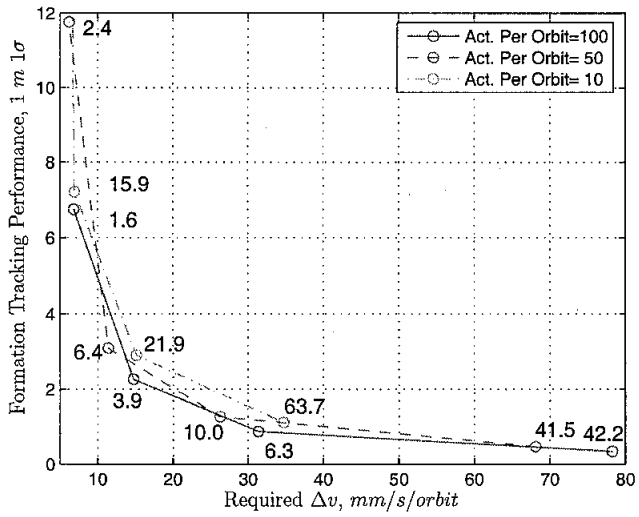

Figure 2. L/F Δv Requirements for Varying Performance Levels with Actuation Period of 0.1 s.

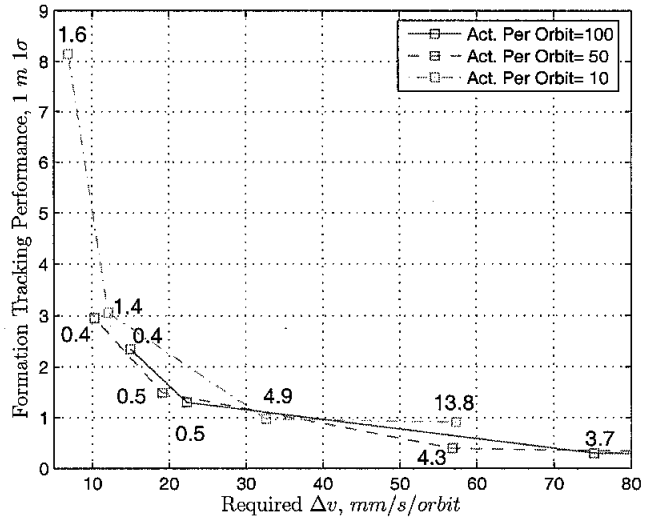

Figure 3. L/F Δv Requirements for Varying Performance Levels with Actuation Period of 1.0 s.

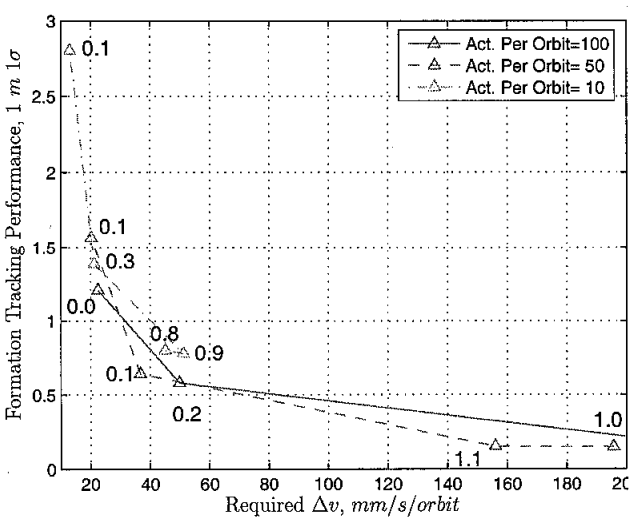

Figure 4. L/F Δv Requirements for Varying Performance Levels with Actuation Period of 10.0 s.

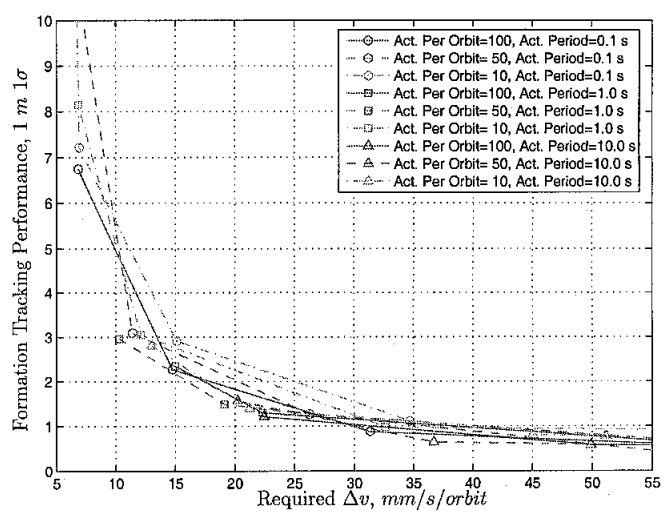

Figure 5. L/F Δv Requirements for Varying Performance Levels for All Actuation Periods.

Table 4: Δv Requirements in $mm/s/$orbit by Architecture.

	L/F	COF	IVS
10 $m\,1\sigma$ Perf.	6.8	5.8	1.4
5 $m\,1\sigma$ Perf.	9.9	10.5	2.2
1 $m\,1\sigma$ Perf.	29.9	23.7	8.2
0.1 $m\,1\sigma$ Perf.	219.1	186.3	32.6

to their $1\,\sigma$ values yields a Δv of 11.8 $mm/s/orbit$. We hypothesize that the remaining difference is due to either the better performance of the model predictive controller or the method by which the desired true anomaly is specified in the previous study.

IVS maintains 10 m absolute performance for 3.7 $mm/s/orbit$. This is a 46% improvement over the previously best reported value of 6.9 $mm/s/orbit$. The drawback is that there is no stability proof for IVS.

6. CONCLUSIONS

The principal result of this study is that IVS is currently the most efficient formation control architecture for Earth-orbiting formations: $10\,m$ absolute relative position control can be maintained for approximately 4 $mm/s/orbit$ and $0.3\,m$ absolute relative position control can be maintained for approximately 33 $mm/s/orbit$.

Future work includes developing stability proofs for IVS, incorporating a quantized thrust model in the simulation environment, and developing better methods for specifying the desired true anomaly for the COF and L/F architectures. The specification of the desired trajectories is what drives formation Δv requirements. IVS is the most efficient because it does not follow a prescribed desired profile, but fits a desired prescribed formation shape to the current formation state.

The reason to continue studying methods for improving the performance of the L/F architecture is that it is currently one of the few architectures with guaranteed stability. To parameterize the desired trajectories for the L/F and COF architectures we used the true anomaly of a Keplerian reference orbit based on the instantaneous, noise-corrupted orbital elements of the reference spacecraft, updated each orbit. Related work has used mean orbital elements to control formations in the presence of Earth oblateness.[23] Using the true anomaly of the *mean* orbit of the reference spacecraft as the desired true anomaly may be more advantageous.

7. APPENDIX

The discretized control model is based on the closed-form state transition matrix of (8) with state $[\,x\ y\ z\ \dot{x}\ \dot{y}\ \dot{z}\,]^T$. In the following, t is used for the sample period and

$$\alpha_1 = \frac{2-5c^2}{2-c^2} \quad \alpha_2 = \frac{4c^2}{2-c^2} \quad \alpha_3 = \frac{2c}{(2-c^2)n} \quad \gamma_1^2 = (2-c^2)n^2 \quad \gamma_2^2 = (3c^2-2)n^2$$

$$C_i = \cos(\gamma_i t) \quad S_i = \sin(\gamma_i t) \quad C_i^\sigma = \cos(\gamma_i t(1-\sigma)) \quad S_i^\sigma = \sin(\gamma_i t(1-\sigma))\,.$$

Then,

$$e^{At} = \begin{bmatrix} \alpha_1 C_1 + \alpha_2 & 0 & 0 & S_1/\gamma_1 & \alpha_3(1-C_1) & 0 \\ 2nc\alpha_1(t - S_1/\gamma_1) & 1 & 0 & -\alpha_3(1-C_1) & \alpha_1 t + \alpha_2 C_1/\gamma_1 & 0 \\ 0 & 0 & C_2 & 0 & 0 & S_2/\gamma_2 \\ -\gamma_1\alpha_1 S_1 & 0 & 0 & C_1 & \gamma_1\alpha_3 S_1 & 0 \\ 2nc\alpha_1(1-C_1) & 0 & 0 & -\alpha_3\gamma_1 S_1 & \alpha_1 + \alpha_2 C_1 & 0 \\ 0 & 0 & -\gamma_2 S_2 & 0 & 0 & C_2 \end{bmatrix} \tag{12}$$

and

$$B_d = \begin{bmatrix} (C_1^\sigma - C_1)/\gamma_1^2 & \alpha_3(\sigma t - (S_1 - S_1^\sigma)/\gamma_1) & 0 \\ -\alpha_3(\sigma t - (S_1 - S_1^\sigma)/\gamma_1) & \alpha_1 \sigma t^2(1-\sigma/2) + \alpha_2(C_1^\sigma - C_1)/\gamma_1^2 & 0 \\ 0 & 0 & (C_2^\sigma - C_2)/\gamma_2^2 \\ (S_1 - S_1^\sigma)/\gamma_1 & \alpha_3(C_1^\sigma - C_1) & 0 \\ -\alpha_3(C_1^\sigma - C_1) & \alpha_1 \sigma t + \alpha_2(S_1 - S_1^\sigma)/\gamma_1 & 0 \\ 0 & 0 & (S_2 - S_2^\sigma)/\gamma_2 \end{bmatrix}. \tag{13}$$

ACKNOWLEDGMENTS

This research was performed at the Jet Propulsion Laboratory, California Institute of Technology, under contract with the National Aeronautics and Space Administration.

REFERENCES

1. H. Fiedler and G. Krieger, "Close formation of micro-satellites for SAR interferometry," in *2nd Int. Symp. on Formation Flying Missions & Technologies*, 2004.
2. E. Kong, D. Miller, and R. Sedwick, "Exploiting orbital dynamics for aperture synthesis using distributed satellite systems: Applications to a visible earth imager system," *Journal of the Astronautical Sciences* **47**(1), pp. 53–75, 1999.
3. D. Scharf, S. Ploen, F. Hadaegh, J. Keim, and L. Phan, "Guaranteed initialization of distributed spacecraft formations," in *Proceedings of the AIAA Guidance, Navigation,&Control Conference*, 2003.
4. M. Tillerson and J. How, "Advanced guidance algorithms for spacecraft formation-keeping," in *Proceedings of the American Control Conference*, pp. 2830–2835, 2002.
5. M. Tillerson, L. Breger, and J. How, "Distributed coordination and control of formation flying spacecraft," in *Proceedings of the American Control Conference*, pp. 1740–1645, 2003.
6. D. Scharf, F. Hadaegh, and S. Ploen, "A survey of spacecraft formation flying guidance and control (Part II): Control," in *Proceedings of the American Control Conference*, 2004.
7. T. Balch and R. Arkin, "Behavior-based formation control for multirobot teams," *IEEE Transactions on Robotics and Automation* **14**(6), pp. 926–939, 1998.
8. M. Tillerson, G. Inalhan, and J. How, "Co-ordination and control of distributed spacecraft systems using convex optimization techniques," *International Journal of Robust & Nonlinear Control* **12**(2,3), pp. 207–242, 2002.
9. P. Stadter, A. Chacos, R. Heins, G. Moore, E. Olsen, and M. Asher, "Confluence of navigation, communication and control in distributed spacecraft systems," *IEEE Aero. and Elec. Sys. Mag.* **17**(5), pp. 26–32, 2002.
10. T. Corazzini, A. Robertson, J. Adams, A. Hassibi, and J. How, "Experimental demonstration of GPS as a relative sensor for formation flying spacecraft," *J. of the Institute of Navigation* **45**(3), pp. 195–207, 1998.
11. W. Clohessy and R. Wiltshire, "Terminal guidance system for satellite rendezvous," *J. Aerospace Sci.* **27**(9), pp. 653–658,674, 1960.
12. H.-H. Yeh and A. Sparks, "Geometry and control of satellite formations," in *Proceedings of the American Control Conference*, 2002.
13. J. Prussing and B. Conway, *Orbital Mechanics*, Oxford University Press, New York, New York, 1993.
14. D. Scharf, S. Ploen, and F. Hadaegh, "A survey of spacecraft formation flying guidance and control (Part I): Guidance," in *Proceedings of the American Control Conference*, 2003.
15. G. Inalhan, M. Tillerson, and J. How, "Relative dynamics and control of spacecraft formations in eccentric orbits," *Journal of Guidance, Control, and Dynamics* **25**(1), pp. 48–59, 2002.
16. F. Lewis, *Optimal Control*, John Wiley & Sons, New York, New York, 1986.
17. S. Schweighart and R. Sedwick, "High-fidelity linearized J_2 model for satellite formation flight," *Journal of Guidance, Control, and Dynamics* **25**(6), pp. 1073–1080, 2003.
18. F. Hadaegh, A. Ghavimi, G. Singh, and M. Quadrelli, "A centralized optimal controller for formation flying spacecraft," in *Int. Conf. Intel. Tech.*, 2000.

19. R. Smith and F. Hadaegh, "Control topologies for deep space formation flying spacecraft," in *Proceedings of the American Control Conference*, pp. 2836–2841, 2002.
20. P. Wang, "Navigation strategies for multiple autonomous mobile robots moving in formation," *Journal of Robotic Systems* **8**(2), pp. 177–195, 1991.
21. F. Bauer, K. Hartman, and E. Lightsey, "Spacebourne GPS current status and future visions," in *Proceedings of the IEEE Aerospace Conference*, 1998.
22. F. Busse and J. How, "Real-time experimental demonstration of precise decentralized relative navigation for formation flying spacecraft," in *Proceedings of the AIAA Guidance, Navigation,&Control Conference*, 2002.
23. H. Schuab, S. Vadali, J. Junkins, and K. Alfriend, "Spacecraft formation flying using mean orbital elements," *Journal of the Astronautical Sciences* **48**(1), pp. 69–87, 1999.